Supporting Information: Fast and Versatile Thermo-osmotic Flows with a Pinch of Salt

Cecilia Herrero,[†] Michael de San Féliciano,[†] Samy Merabia,[*,†] and Laurent Joly[*,†,‡]

†*Univ Lyon, Univ Claude Bernard Lyon 1, CNRS, Institut Lumière Matière, F-69622, VILLEURBANNE, France*

‡*Institut Universitaire de France (IUF), 1 rue Descartes, 75005 Paris, France*

E-mail: samy.merabia@univ-lyon1.fr; laurent.joly@univ-lyon1.fr

Contents

1 Analytical framework derivation

With the final objective of obtaining an analytical expression for the different contributions to the total thermo-osmotic response, we developed a general model to include the additional contributions to the enthalpy excess density δh related to the solvent and the ions, along with the electrostatic enthalpy of ions δh_{el} considered by the standard approach.[S1,S2] All the quantities were computed within the Poisson-Boltzmann framework. Details on such framework and its range of validity are discussed in Ref. S3.

1.1 Hydrodynamic boundary condition and osmotic velocity profile

The standard no-slip boundary condition (BC), which supposes that the fluid velocity vanishes when in contact to the wall, needs to be refined at the nanoscale. Two different situations can occur. First, we can consider the presence of a liquid stagnant layer close to the wall (Fig. S1, $b_{\mathrm{eff}} = b - z_{\mathrm{s}} < 0$), implying a vanishing velocity profile inside the channel. The typical size of the stagnant layer, due to the layering of the fluid close to the wall, is of order of one molecular diameter,[S4] $\sigma \sim 2.75\,\text{Å}$ for water. In this case, $-b_{\mathrm{eff}}$ identifies with the size of

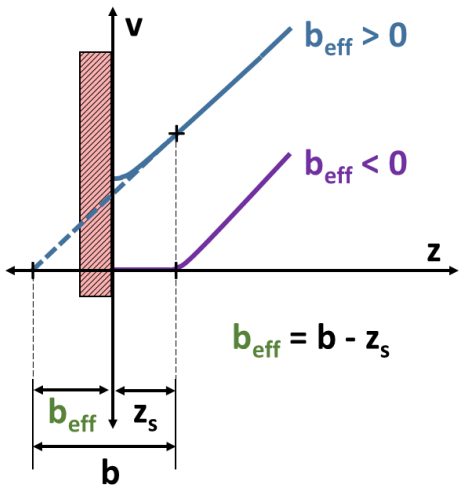

Figure S1: Schematics of the effective slip length b_{eff} as a function of the slip length b and the shear plane position z_{s}.

the stagnant layer present at the liquid-solid interface,
where the liquid velocity vanishes.

Second, we can consider an interfacial velocity jump (Fig. S1 with $b_{\text{eff}} = b - z_{\text{s}} > 0$), also known as slip velocity v_{s}, described via the partial slip BC:

$$v_{\text{s}} = b \left. \frac{\partial v}{\partial z} \right|_{z=z_{\text{s}}}, \tag{1}$$

where z_{s} corresponds to the shear plane position and b is the slip length (with $b = \eta/\lambda$, η being the shear viscosity and λ the liquid-solid friction coefficient). This BC becomes critical to take it into account at the nano- and micro-metric scales, due to the typical order of magnitude of the slip length, $b \sim 10^0 - 10^2\,\text{nm}$.[S5–S7]

In terms of wettability, we can expect the presence of a stagnant layer in the most hydrophilic systems, where the liquid molecules have more tendency to accumulate close to the wall, while a slipping system will correspond to hydrophobic interfaces, with small liquid-solid friction coefficient due to the weaker interactions with the wall.

The appropriate boundary conditions together with the Stokes equation

$$-\eta \Delta v = -\nabla p + f_{\text{ext}}, \tag{2}$$

where p is the pressure and f_{ext} is an applied external force per unit volume, allow us to derive a general expression for the osmotic velocity profile close to a planar wall as a function of the force density profile in the interaction layer. Let us first simplify Eq. (2) by considering $f = -\nabla p + f_{\text{ext}}$ the force density generated by the thermodynamic gradients in the interfacial layer. Integrating Stokes Eq. (2), in the lubrication limit and supposing force and therefore velocity derivative vanish far from the wall, we obtain:

$$-\eta \frac{\partial v_x(z)}{\partial z} = \int_{+\infty}^{z} f(z')\,\mathrm{d}z'. \tag{3}$$

Integrating again between the position z_0 (with $z_0 = 0$ in the slip case, and $z_0 = -b_{\text{eff}}$ in the stagnant layer case; see Fig. S1) and z, we obtain:

$$v_x(z) - v_x(z_0) = \int_{z_0}^{z} \mathrm{d}z' \int_{z'}^{\infty} \frac{1}{\eta} f(z'')\, \mathrm{d}z''. \tag{4}$$

We can replace $v_x(z_0)$ by the relevant BC from Eq. (1) (with $b = 0$ in the stagnant layer situation) obtaining:

$$v_x(z) = \frac{1}{\eta}\left[\int_{z_0}^{z} \mathrm{d}z' \int_{z'}^{\infty} f(z'')\, \mathrm{d}z'' + (b_{\text{eff}} + z_0) \int_{z_0}^{\infty} f(z)\, \mathrm{d}z\right]; \tag{5}$$

which reduces, integrating by parts and taking the velocity limit far from the wall, to:

$$v_{\text{osm}}^{\infty} = \lim_{z\to\infty} v_x(z) = \frac{1}{\eta} \int_{z_0}^{\infty} (z + b_{\text{eff}})\, f(z)\, \mathrm{d}z. \tag{6}$$

The osmotic velocity profile, given by the general expression Eq. (5) far from the wall, is of special interest when computing the different coefficients of the response matrix.

In the case of thermo-osmosis, for instance, it is straightforward to obtain the thermo-osmotic response coefficient M_{tosm}, defined from the relation: $v_{\text{osm}} = M_{\text{to}}(-\nabla T/T)$.[S8] In this case, the force density driving the flow is the thermodynamic force $f = -T\nabla(\mu/T)$ with μ the chemical potential. Taking into account the Gibbs-Helmholtz equation, $\mathrm{d}(\mu/T)/\mathrm{d}T = \delta h/T^2$,[S9] we obtain that

$$f(z) = -\delta h(z) \frac{\nabla T}{T}. \tag{7}$$

Substituting f in Eq. (6) we obtain:

$$v_{\text{osm}}^{\infty} = -\frac{\nabla T/T}{\eta} \int_{z_0}^{\infty} \delta h(z)(z + b_{\text{eff}})\mathrm{d}z. \tag{8}$$

Finally, the thermo-osmotic response coefficient $M_{\text{to}} = v_{\text{osm}}/(-\nabla T/T)$ is given by the general

expression:

$$M_{\mathrm{to}} = \frac{1}{\eta}\int_{z_0}^{\infty} \delta h(z)(z + b_{\mathrm{eff}})\mathrm{d}z. \tag{9}$$

1.2 Enthalpy excess density

The enthalpy excess density δh is a fundamental quantity in Eq. (9). Here we introduce some general concepts related to its classical description,[S1,S2] given only by ionic electrostatic interactions, together with some additional contributions that we will account for in the general model we propose to describe the different interactions that play a role in the enthalpy of an aqueous electrolyte.

1.2.1 Notations and characteristic lengths

Notations –

- inverse thermal energy $\beta = 1/(k_{\mathrm{B}}T)$, with k_{B} the Boltzmann constant amd T the temperature
- absolute ionic charge $q = Ze$ with e the elementary charged and Z the ion valence
- electrostatic potential V
- reduced potential $\phi = \beta q V$
- their value at the wall V_{s} and ϕ_{s}
- ion densities $n_{\pm}$
- charge density ρ_{e}
- solvent dielectric permittivity ε
- salt concentration $n_{\mathrm{s}} = n_+ = n_-$ in the bulk/reservoirs
- surface charge density Σ

Characteristic lengths –

Solvent permittivity ε: Bjerrum length ℓ_B – The Bjerrum length is the distance at which the electrostatic interaction energy between two ions is equal to the thermal energy $k_{\mathrm{B}}T$.

$$\ell_{\mathrm{B}} = \frac{\beta q^2}{4\pi\varepsilon} \quad \Leftrightarrow \quad \varepsilon = \frac{\beta q^2}{4\pi\ell_{\mathrm{B}}} \tag{10}$$

For a monovalent salt in water at room temperature, $\ell_{\mathrm{B}} \sim 0.7\,\mathrm{nm}$.

Bulk salt concentration n_0: Debye length λ_D – The Debye length is the range of the exponential screening of the electric field in an electrolyte.

$$\lambda_{\mathrm{D}} = \frac{1}{\sqrt{8\pi\ell_{\mathrm{B}} n_0}} \quad \Leftrightarrow \quad n_0 = \frac{1}{8\pi\ell_{\mathrm{B}}\lambda_{\mathrm{D}}^2} \tag{11}$$

For a monovalent salt in water at room temperature, $\lambda_{\mathrm{D}} \sim 0.3\,\mathrm{nm}/\sqrt{n_0(\mathrm{mol/L})}$.

Surface charge density Σ: Gouy-Chapman length ℓ_{GC} – The Gouy-Chapman length is the distance at which the electrostatic interaction energy between an ion and a charged surface is comparable to the thermal energy $k_{\mathrm{B}}T$.

$$\ell_{\mathrm{GC}} = \frac{q}{2\pi\ell_{\mathrm{B}}|\Sigma|} \quad \Leftrightarrow \quad \Sigma = \mathrm{sgn}(\Sigma)\frac{q}{2\pi\ell_{\mathrm{B}}\ell_{\mathrm{GC}}} \tag{12}$$

For monovalent ions in water at room temperature, $\ell_{\mathrm{GC}} \sim 36\,\mathrm{nm}/|\Sigma|(\mathrm{mC/m^2})$.

In the following, it will appear that many quantities can be expressed as a function of the ratio $\lambda_{\mathrm{D}}/\ell_{\mathrm{GC}}$, which is proportional to the absolute value of the surface charge, and inversely proportional to the square root of the bulk salt concentration:

$$\frac{\lambda_{\mathrm{D}}}{\ell_{\mathrm{GC}}} = 2\pi\ell_{\mathrm{B}}\lambda_{\mathrm{D}}\frac{|\Sigma|}{q} = \frac{|\Sigma|/q}{\sqrt{n_0}}\sqrt{\frac{\pi\ell_{\mathrm{B}}}{2}}$$

1.2.2 General remarks

In the case of aqueous electrolytes, originally, Derjaguin et al. developed a model for the thermo-osmotic coefficient[S1,S2] as in Eq. (9) without the slip term, and only considering the electrostatic enthalpy of the ions $\delta h_{\rm el}(z) = \rho_{\rm e}(z)V(z)+p(z)$. By taking into account Poisson's equation[S3] and considering mechanical equilibrium along the z direction $\left(\frac{{\rm d}p}{{\rm d}z} = -\rho_{\rm e}\frac{{\rm d}V}{{\rm d}z}\right)$, we obtain an expression of $\delta h_{\rm el}$ as a function of the electric potential:

$$\delta h_{\rm el}(z) = -\varepsilon V(z)\frac{{\rm d}^2V}{{\rm d}z^2} + \frac{\varepsilon}{2}\left(\frac{{\rm d}V}{{\rm d}z}\right)^2. \tag{13}$$

Just focusing on this classical theory,[S2] which only considers the electrostatic interactions between ions ($\delta h \simeq \delta h_{\rm el}$), substituting Eq. (13) in Eq. (9), we can solve the integral analytically in the slip situation, obtaining the electrostatic constribution to the thermo-osmotic response as a function of the ratio $x = \lambda_{\rm D}/\ell_{\rm GC}$ (see Section 1.2.1):

$$M_{\rm to}^{\rm el} = \frac{1}{2\pi\ell_{\rm B}\eta\beta}\left\{-3\ln\left(1-\gamma^2\right) - {\rm asinh}^2(x) + \frac{b_{\rm eff}}{\lambda_{\rm D}}\left[3x|\gamma| - 2x\,{\rm asinh}(x)\right]\right\}, \tag{14}$$

with

$$\gamma = \tanh\left(\frac{\phi_{\rm s}}{4}\right) = \frac{{\rm sgn}(\Sigma)}{x}\left(-1+\sqrt{1+x^2}\right). \tag{15}$$

This expression can be simplified in the Debye-Hückel regime, which was the one considered by Derjaguin,[S1,S2] then $x \ll 1$:

$$M_{\rm to}^{\rm el,DH} = -\frac{x^2}{8\pi\ell_{\rm B}\eta\beta}\left(1+2\frac{b_{\rm eff}}{\lambda_{\rm D}}\right), \tag{16}$$

and thus scaling as Σ^2 in this regime. A different scaling with x is found for high surface charges, *i.e.* when $x \gg 1$, when the contribution is given by the expression:

$$M_{\rm to}^{{\rm el},x\gg1} = \frac{1}{2\pi\ell_{\rm B}\eta\beta}\left\{3\ln\left(\frac{x}{2}\right) - \ln^2(2x) + \frac{b_{\rm eff}}{\lambda_{\rm D}}x\left[3-2\ln(2x)\right]\right\}. \tag{17}$$

It is interesting to note that none of these expressions depend on the sign of the surface charge: M_{to} is always negative.

Although the model proposed by Derjaguin et al. is useful to quantitatively predict some M_{to} experimental orders of magnitude,[S9] it fails to describe the amplitude of the responses predicted in the literature,[S8,S10–S12] the thermo-osmotic response reported for weakly charged membranes,[S13] as well as the experimental discrepancies observed in M_{to} sign.[S9,S14–S16] Although electrostatic ionic interactions are for sure an important ingredient controlling the thermodynamical processes of a dissolved salt in a charged channel, other interactions discarded by the classical model may also be critical to describe thermo-osmosis, such as the liquid-solid interactions (*i.e.* the wetting properties), as well as the ion specificity[S17].

Generally, the atomic enthalpy excess density for an element i can be defined as:

$$\delta h_i(z) = \left[\delta u_i(z) + \delta p_i(z)\right] n_i(z), \tag{18}$$

where $\delta\mathcal{A}(z) = \mathcal{A}(z) - \mathcal{A}_{\mathrm{bulk}}$; with $\mathcal{A}_{\mathrm{bulk}}$ the bulk value of the physical property $\mathcal{A}$, u_i the energy per atom, p_i the stress per atom [1], and n_i the atomic number density profile. When working at constant temperature, the kinetic energy per atom $u_{\mathrm{k},i}$ is proportional to $k_{\mathrm{B}}T$ for all z, so $\delta u_{\mathrm{k},i} = 0$ and $\delta u_i = \delta u_{\mathrm{p},i}$ with $u_{\mathrm{p},i}$ the potential energy per atom.

Equation (18) can be easily extended to the case of molecular fluids as the sum of the different atomic contributions. Therefore, in the case of water:

$$\delta h_{\mathrm{wat}}(z) = \delta h_{\mathrm{O}}(z) + \delta h_{\mathrm{H}}(z). \tag{19}$$

In this case δh_{wat} does not have a simple analytical form and, due to its strong dependence on the wetting properties,[S8,S10] it has to be computed numerically from simulations for a given wall type.

Note that other enthalpy excess density contributions could be considered. Such is the

[1] A practical difficulty with measuring this term will be discussed in Section 3.2.

case of the one associated to the water molecules dipole moment in the EDL given by the expression:

$$\delta h_{\mathrm{dp}}(z) = -\left\langle \mu \right\rangle (z)\, n_{\mathrm{O}}(z)\, E(z), \tag{20}$$

with n_{O} the number density of the oxygen atoms, $E = -\frac{\mathrm{d}V}{\mathrm{d}z}$ the electrostatic field, and $\langle \mu \rangle$ the average dipole moment in the direction of the field. $\langle \mu \rangle$ can be computed from Boltzmann statistics, by taking into account that $\left\langle \mu \right\rangle (z) = \mu \left\langle \cos\theta \right\rangle (z)$, with $\langle \cos\theta \rangle$ the average dipole moment orientation and μ the dipole moment of the solvent, $\mu = 1.85$ D for water. With that regard, denoting $\mathcal{P}_{\mathrm{B}}$ the probability that the molecule will have the angle θ, then

$$\mathcal{P}_{\mathrm{B}} = \frac{e^{\alpha \cos\theta}}{\int \mathrm{d}\Omega\, e^{\alpha \cos\theta}}, \tag{21}$$

where Ω is the solid angle and $\alpha = \beta \mu E$. Therefore,

$$\left\langle \mu \right\rangle = \int \mathrm{d}\Omega\, \mu\, \mathcal{P}_{\mathrm{B}} \cos\theta = \frac{\mu \int_0^{\pi} e^{\alpha \cos\theta} \cos\theta \sin\theta\, \mathrm{d}\theta}{\int_0^{\pi} e^{\alpha \cos\theta} \sin\theta\, \mathrm{d}\theta} = \mu \left(\coth\alpha - \frac{1}{\alpha} \right). \tag{22}$$

By linearizing this expression when $\mu E \ll k_{\mathrm{B}} T$ and substituting in Eq. (20) we finally obtain:

$$\delta h_{\mathrm{dp}}(z) = -\frac{1}{3\beta} \left(\frac{\mu}{q} \right)^2 n_{\mathrm{O}}(z) \left(\frac{\mathrm{d}\phi}{\mathrm{d}z} \right)^2, \tag{23}$$

where ϕ is the reduced potential (see Section 1.2.1). We can obtain n_{O} from molecular dynamics simulations and $\phi(z)$ solving the Poisson-Boltzmann equation[S3] for the corresponding geometry.

One of the objectives of the present work is to introduce a general model that accounts for the different interactions taking place in a liquid electrolyte, namely the solute and solvent electrostatic interactions (in the presence of a charged surface) and purely neutral interactions (due to the solid wetting properties).

1.2.3 Proposed model

The main idea in the model we propose here is, following the ideas of Ref. S18, to include the additional contributions to δh related to the solvent (water in the present work) and the ions, along with the electrostatic enthalpy of ions δh_{el} considered by the standard approach.

The **water contribution** in the case of a neutral surface ($\Sigma = 0$), will be given by the sum of the oxygen and hydrogen atomic enthalpies, which can be directly determined from equilibrium MD simulations following Eqs. (18) and (19), so $\delta h^0_{\mathrm{wat}} = \delta h^0_{\mathrm{O}} + \delta h^0_{\mathrm{H}}$. In the case of a charged surface Σ, we should also account for the dipole moment contribution, $\delta h^{\Sigma}_{\mathrm{dp}}$ from Eq. (23), writing the total water enthalpy contribution as $\delta h^0_{\mathrm{wat}} + \delta h^{\Sigma}_{\mathrm{dp}}$.

Analogously, the **ions contribution** for a neutral surface will write $\delta h^0_{\mathrm{ions}} = \delta h^0_+ + \delta h^0_-$, where

$$\delta h^0_{\pm} = \left(\delta u^0_{\pm} + \delta p^0_{\pm}\right) n^0_{\pm}, \tag{24}$$

with the ions distribution given by an exponential of the potential energy variation; for symmetric salts depleted from the wall:

$$n^0_{\pm} = n^0_{\mathrm{s}} \exp\left(-\beta \delta u^0_{\pm}\right); \tag{25}$$

$n^0_{\pm}$ can also be determined from equilibrium MD simulations at a reference bulk concentration n^0_{s}.

We can extend this description to a charged surface, by including the potential (described within the Poisson-Boltzmann framework) in Eq. (24):

$$\delta h^{\Sigma}_{\mathrm{ions}} = \left(\delta u^0_+ + \delta p^0_+ + qV\right) n^{\Sigma}_+ + \left(\delta u^0_- + \delta p^0_- - qV\right) n^{\Sigma}_-; \tag{26}$$

where the ionic concentrations will be given by the Boltzmann distribution:

$$n^{\Sigma}_{\pm} = n_{\mathrm{s}} \exp\left[-\beta\left(\delta u^0_{\pm} \pm qV\right)\right] = n_{\pm} \exp\left(-\beta \delta u^0_{\pm}\right), \tag{27}$$

with $n_\pm$ the ion distributions within the Poisson-Boltzmann framework, given by the Boltzmann equation.[S3] Rearranging terms in Eq. (26) we obtain:

$$\begin{aligned}\delta h^{\Sigma}_{\text{ions}} &= \frac{\delta h^0_+}{n^0_{\text{s}}} n_+ + \frac{\delta h^0_-}{n^0_{\text{s}}} n_- + q\left(n^{\Sigma}_+ - n^{\Sigma}_-\right) V \\ &= \delta h^{\Sigma}_{\text{sol}} + \delta h^{\Sigma}_{\text{mix}} + \delta h^{\Sigma}_{\text{ES}},\end{aligned} \tag{28}$$

from where we defined the solvation enthalpy as the enthalpy contribution from the first two terms:

$$\delta h^{\Sigma}_{\text{sol}} = \frac{\delta h^0_+}{n^0_{\text{s}}} n_+ + \frac{\delta h^0_-}{n^0_{\text{s}}} n_-. \tag{29}$$

The potential term in Eq. (28) is in turn decomposed into a purely electrostatic contribution:

$$\delta h^{\Sigma}_{\text{ES}} = q\left(n_+ - n_-\right) V, \tag{30}$$

and a mixed term

$$\delta h^{\Sigma}_{\text{mix}}(z) = q\left[n_+\left(\frac{n^0_+}{n^0_{\text{s}}} - 1\right) - n_-\left(\frac{n^0_-}{n^0_{\text{s}}} - 1\right)\right] V, \tag{31}$$

which acts as a compensation term for $\delta h^{\Sigma}_{\text{ES}}$ in the region where the ions are depleted from the wall. Indeed, when the salts are depleted from the wall (typically symmetric salts), their density profile for neutral walls can be approximated by a step function with $n^0_\pm = n^0_{\text{s}}$ in bulk and $n^0_\pm = 0$ close to the wall, so $\delta h^{\Sigma}_{\text{mix}} = 0$ in bulk and $\delta h^{\Sigma}_{\text{mix}} = -\delta h^{\Sigma}_{\text{ES}}$ at the interface.

A full picture will be completed by considering the electrostatic pressure contribution $\delta p^{\Sigma}_{\text{ES}} = \frac{\varepsilon}{2}\left(\frac{\mathrm{d}V}{\mathrm{d}z}\right)^2$ which, together with $\delta h^{\Sigma}_{\text{ES}}$, form the classical electrostatic term from Eq. (13), $\delta h_{\text{el}} = \delta h^{\Sigma}_{\text{ES}} + \delta p^{\Sigma}_{\text{ES}}$. In conclusion, dropping the enthalpies super indexes related to the surface charge in order to light notation, the total enthalpy excess density writes:

$$\delta h(z) = \delta h_{\text{wat}}(z) + \delta h_{\text{dp}}(z) + \delta h_{\text{sol}}(z) + \delta h_{\text{mix}}(z) + \delta h_{\text{el}}(z). \tag{32}$$

Finally, we denote $\delta h^*_{\rm el} \approx \delta h_{\rm mix} + \delta h_{\rm el}$, with

$$\delta h^*_{\rm el} = \begin{cases} \delta h_{\rm el} & \text{for } z > d_\ell \\ 0 & \text{for } z \leq d_\ell \end{cases}, \tag{33}$$

where d_ℓ corresponds to the characteristic length corresponding to the depletion of the ions from the wall. Therefore the total enthalpy can be expressed as:

$$\delta h(z) = \delta h_{\rm wat}(z) + \delta h_{\rm sol}(z) + \delta h_{\rm dp}(z) + \delta h^*_{\rm el}(z). \tag{34}$$

In this equation we can distinguish a contribution related to the solvent (water in this work) $\delta h_{\rm wat}$, another one related to the ion solvation $\delta h_{\rm sol}$, and two electrostatic contributions, $\delta h_{\rm dp}$ and $\delta h^*_{\rm el}$, related to the solvent and the ions electrostatic interactions respectively.

2 Molecular dynamics simulations details

We used the LAMMPS package[S19] to determine the enthalpy excess density profiles from equilibrium molecular dynamics (EMD) simulations of an aqueous electrolyte constituted by 2080 water molecules, simulated with the SPC/E water model,[S20] and 80 ions (40 anions and 40 cations) of three different salt types, NaCl, KCl and NaI, such as the bulk salt concentration was $n_{\rm s} \sim 1\,{\rm M}$, following Ref. S21. In this paper, the authors performed MD simulations to study electro-osmotic flow in hydrophobic channels and proposed a theoretical model, extended in Ref. S17, in good agreement with their simulation results. Therefore, we intended to reproduce their system in order to study thermo-osmotic flows. All atomic interactions were modeled with a Lennard-Jones potential characterized by an interaction energy ε_{ij} and size σ_{ij}. The system parameters were the ones indicated in Ref. S21, namely the water-ions interactions were taken from[S22] except for the biggest ion, I^-, for which we considered $\sigma_{\rm II} = 6.00\,{\rm \AA}$.[S17,S21] We imposed periodic boundary conditions in the x and y directions par-

allel to the walls with lateral sizes $L_x = 48.21\,\text{Å}$ and $L_y = 32.14\,\text{Å}$. The structure of the walls consisted in three atomic layers structured as a face centered cubic crystal exhibiting a (001) face to the fluid, with a lattice parameter $a = 5.356\,\text{Å}$. The solid wall atoms were frozen and the oxygen-solid (LS) interactions were varied between the hydrophobic and hydrophilic values given in Ref. S21, with $\varepsilon_{\text{SS}} = \{0.164, 0.343, 0.673, 1.113, 2.08\}$ kcal/mol. These wettings are characterized by the respective contact angles $\theta \sim \{140°, 130°, 110°, 90°, 50°\}$, determined from additional sessile drop simulations on uncharged surfaces (where we followed the procedure detailed in Ref. S18). The values for the contact angles, measured at 298 K from three independent simulations for a given wetting, can be found in Table S1. Lorentz-Berthelot mixing rules were applied for all the cross-interactions.

For all the simulations we imposed a timestep of 2 fs and we ran an equilibration stage of 500 ps where we fixed the temperature at 298 K via a Nosé-Hoover thermostat with a damping time of 200 fs. Following Ref. S21, we also set the pressure to 10 atm by using the top wall as a piston. We then continued applying the thermostat, and fixed the top wall at its equilibrium position in the production run. The average distance between the walls for all the runs was $\tilde{H} \sim 45$ Å.

The slip length was determined from non-equilibrium molecular dynamics (NEMD) simulations of 1 M of NaCl dissolved in SPC/E water at 10 atm. With that regard, we applied a constant shear velocity U_{wall} to both walls in opposite x directions, generating far from the wall a linear velocity profile with constant shear rate. The friction coefficient was determined from the relation $\tau = \lambda v_{\text{s}}$ between the shear stress τ and the velocity jump at the interface, $v_{\text{s}} = U_{\text{wall}} - v_x(z_{\text{s}})$, with z_{s} measured from the Gibbs dividing plane method, see Ref. S4. The slip length was then $b = \eta/\lambda$, with η corresponding to the bulk viscosity obtained from the relation $\tau = \eta \frac{\mathrm{d}v_x}{\mathrm{d}z}$.

For a given wetting angle, determined by ε_{LS}, 3 independent shears in the linear response regime were applied, $U_{\text{wall}} = \{10, 15, 20\}$ m/s, and for a given shear three independent simulations were performed, giving (taking into account the possibility of independently

measuring τ for the top and the bottom wall) 18 independent measures of viscosity and friction, with a production time of 4 ns. The error of both transport coefficients corresponded to the statistical error within 95% of confidence level and the error on b was determined from error propagation computation:

$$\Delta b = b\sqrt{\left(\frac{\Delta\eta}{\eta}\right)^2 + \left(\frac{\Delta\lambda}{\lambda}\right)^2}. \tag{35}$$

Good agreement was found between the simulated viscosity and the experimental value for all the wettings.[S23,S24] The slip length and shear plane position values are shown in Table S1, where we note that the most hydrophilic situation ($\theta \sim 50°$) is a no-slip situation with $b = 0.0$ Å.

Table S1: Slip length b and shear plane position z_s along with the effective slip $b_{\text{eff}} = b - z_s$, for the different wetting angles θ considered in our study, which are controlled by the interaction energy ε_{LS} between liquid and solid atoms

θ (deg)	ε_{LS} (kcal/mol)	b (Å)	z_s (Å)	b_{eff} (Å)
142.16 ± 16.49	0.160	54.89 ± 6.99	1.44 ± 0.02	53.45
127.90 ± 6.20	0.231	23.50 ± 1.82	1.07 ± 0.06	22.43
108.41 ± 0.81	0.323	6.94 ± 2.05	0.83 ± 0.05	6.11
87.25 ± 8.29	0.416	3.98 ± 0.53	0.59 ± 0.13	3.39
51.46 ± 2.65	0.568	0.0 (-0.47 ± 0.34)	0.33 ± 0.03	-0.33

Aside of EMD and NEMD simulations of different aqueous electrolytes enclosed between LJ walls, we also performed an extra set of simulations of 1 M of NaCl dissolved in SPC/E water confined between graphene walls with size $L_x = 46.73$ Å and $L_y = 34.08$ Å. The solution parameters were the same than the ones for LJ walls and the oxygen-carbon interactions were modelled as described in Ref. S25, with a contact angle of $\theta = 84.98° \pm 5.57°$. The slip length of this configuration, measured analogously as for LJ walls, was $b = 539.53 \pm 41.23$ Å and $z_s = 0.76 \pm 0.20$ Å.

3 Generality of the proposed model

After exposing the theroretical framework under which we will obtain the different contributions to $M_{\rm to}$, we also detailed the MD simulations we performed with the objective of determining the solvent and solute atomic enthalpies as a function of the wetting properties of the system. MD simulations are a useful and necessary tool to obtain such atomic enthalpy profiles, although they present some limitations that are discussed here.

3.1 Enthalpy excess density determination

The only contributions to δh in Eq. (34) that cannot be computed analytically are the solvent and solvation contributions, $\delta h_{\rm wat}$ and $\delta h_{\rm sol}$ respectively. In Fig. S2 we can find represented the total enthalpy excess densities computed directly from the aqueous electrolyte solutions following Eq. (18) for NaCl, KCl (Fig. S2a), and NaI (Fig. S2b), for a concentration $n_{\rm s} = 1\,{\rm M}$, together with the profiles for pure water simulations (with no dissolved ions). In Fig. S2 we can see that in the case of an asymmetric salt, with a large anion which adsorbs specifically on the surface (Fig. S2b), the solute enthalpy density profile presents a non negligible contribution. However, in the case of symmetric salts (Fig. S2a), the solute enthalpy, even at large concentrations, does not affect the total enthalpy profile, which is controlled by the solvent. Therefore, in the following, we will present the different enthalpies results for NaCl dissolved in water within a 1 M concentration, although they are equivalent to pure water simulation results and thus extendable to any other symmetric salt type and lower concentrations.

The fact that the solution profile is mostly dominated by water is due to the depletion of the ions from the wall, characteristic of symmetric salts, which implies that only the water molecules are affected by the interactions with the solid atoms (Fig. S3). Therefore, we decided to approximate the ion density profiles (in Fig. S3b) by a smooth step function given by, for half the channel, $1/\{1+\exp\big[(d_\ell - x)/(1\ \text{Å})\big]\}$, which allowed us to determine the size of the depletion layer d_ℓ, , typically on the order of ~ 5 Å..

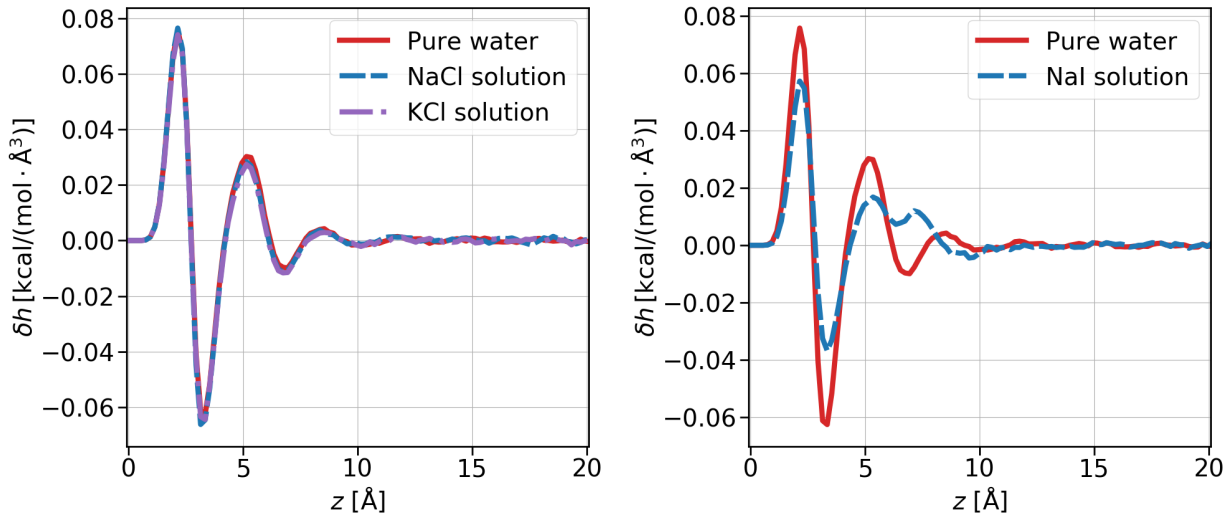

(a) (b)

Figure S2: Enthalpy excess density profiles of pure water (continuous line) simulations together with the profiles corresponding to an aqueous solution of (a) two symmetric salts: NaCl and KCl; and (b) one asymmetric salt: NaI (where the large iodide ion specifically adsorb on the surface), with a bulk salt concentration $n_s \sim 1$ M. All the results correspond to uncharged walls.

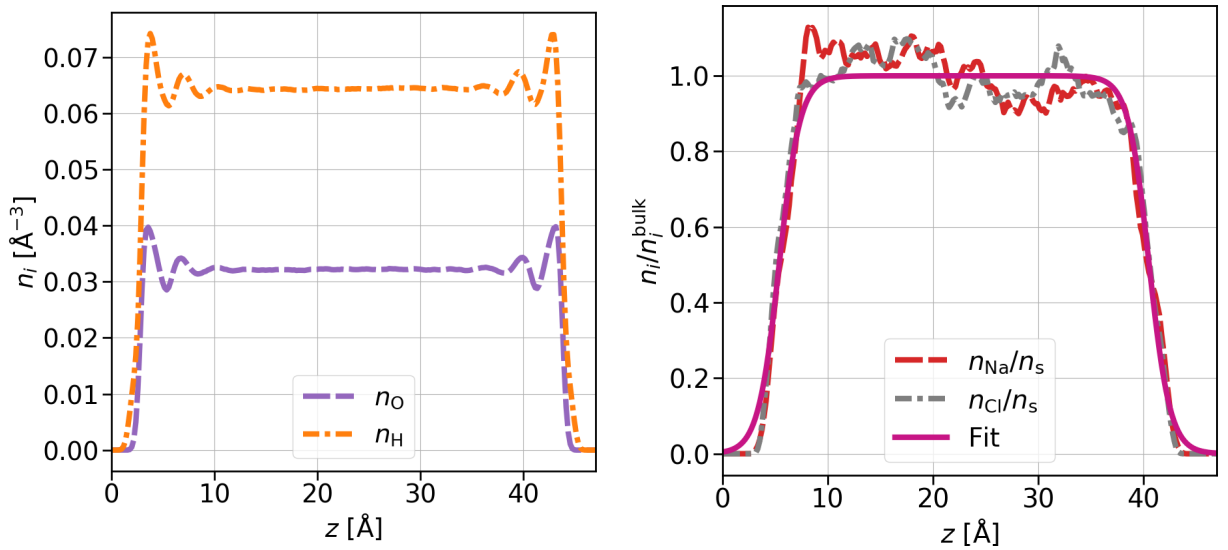

(a) (b)

Figure S3: Number density profiles for an aqueous electrolyte enclosed between LJ walls ($\theta \sim 140°$) of (a) oxygen and hydrogen atoms; (b) Na^+ and Cl^- ions normalized by their bulk concentration n_s. The fit by a smooth step function is also represented in solid line.

3.2 Local pressure profile in MD

Before studying the simulation results, it is important to comment on one important aspect about the enthalpy excess density determination in MD simulations. In the model proposed in Section 3.2 for the enthalpy excess density contributions, we discussed that the enthalpy contributions related to the liquid-solid interactions, namely δh_{wat} and δh_{sol} in Eq. (34), cannot be *a priori* described by a simple analytical formula, and therefore both contributions have to be determined from MD simulations using the atomic enthalpy profiles given by Eq. (18). Nevertheless, in this equation, the enthalpy excess density profile is given as a function of the *local* pressure differences $\delta p(z)$, which are not well defined in molecular dynamics simulations.[S10] Indeed, although the total system pressure is well defined in MD simulations from the total virial of the system,

$$P = nk_{\mathrm{B}}T - \frac{1}{3V}\left\langle \sum_{i<j} \mathbf{r}_{ij} \cdot \mathbf{f}_{ij} \right\rangle, \tag{36}$$

where $n = N/V$ is the density of the system, V its volume, and $\left\langle \sum_{i<j} \mathbf{r}_{ij} \cdot \mathbf{f}_{ij} \right\rangle$ the expected value of the sum of the products of the interparticle distance among atoms and the forces acting on them, the local definition of the stress in a liquid is not unique.[S26] Although it can be proven that the vagueness of the local pressure tensor definition have no effect on physical properties such as the solid-liquid surface tension,[S27] it has been already discussed and showed in previous work that the choice of the local pressure definition affects the computed thermo-osmotic response coefficient M_{to}.[S10] Nevertheless, because it has been shown that the different proposed methods to determine δh, including those based on different local stress gradient definitions, provided relatively similar M_{to} results,[S10,S28] we decided to measure the local enthalpy profile from the stress per atom definition based on the virial formulation, easier to implement in MD simulations and which works well to give a general and qualitative picture in terms of orders of magnitude for the different contributions of the thermo-osmotic response, which is the main objective of the present work.

In the presented results we choose a definition of the stress per atom given by the virial-like expression:

$$p_{\alpha\beta i} = m_i v_{\alpha i} v_{\beta i} + \frac{1}{2} \sum_{j \neq i} r_{\alpha ij} f_{\beta ij}, \tag{37}$$

where $p_{\alpha\beta i}$ denotes the stress tensor component for the atom i in the $\alpha\beta$ direction with $\{\alpha, \beta\} = \{x, y, z\}$. In the following, we will drop the spatial coordinates to light notation. In a MD simulation, the local pressure profile is obtained dividing the space in bins (which for simplicity we will suppose of the same size) and averaging over the $N(z_{\text{bin}})$ particles in the bin:

$$p(z_{\text{bin}}) = \frac{\sum_{i \in \text{bin}} p_i}{N(z_{\text{bin}})}.$$

The total pressure acting on the system will be then given by the sum to all the bins of the average pressure tensor multiplied by the number of particles in the bin:

$$\sum_{\text{bin}} p(z_{\text{bin}}) N(z_{\text{bin}}) = \sum_{\text{bin}} \sum_{i \in \text{bin}} p_i.$$

Taking into account from the equipartition theorem that $m \langle v^2 \rangle = k_{\text{B}} T$, and Eq. (36), it is straightforward that

$$\sum_{\text{bin}} \sum_{i \in \text{bin}} p_i = N k_{\text{B}} T + \frac{1}{2} \left\langle \sum_{i<j} r_{ij} f_{ij} \right\rangle = PV.$$

Note that, explicitly accounting for the spatial coordinates, $\sum_\alpha p_{\alpha\alpha} = 3PV$ in a bulk system. We have then proven that the quantity $\int \delta p \, n \, \mathrm{d}z$ in Eq. (18), and therefore the total enthalpy excess defined as

$$H^0 = \int_0^\infty \delta h \, \mathrm{d}z, \tag{38}$$

is unambiguous and independent of the local pressure definition. Nevertheless, the thermo-

osmotic response coefficient, given by Eq. (9), can be decomposed as

$$M_{\mathrm{to}} = \frac{1}{\eta}\left(\int_{z_0}^{\infty} \delta h(z)\, z \,\mathrm{d}z + b_{\mathrm{eff}} H\right), \tag{39}$$

where

$$H = \int_{z_0}^{\infty} \delta h \,\mathrm{d}z. \tag{40}$$

In the slip situation $H = H^0$ and then it will be well defined. However, the integral of $\delta h\, z$ will depend on the local pressure definition and is only expected to predict the real thermo-osmotic response of the system quantitatively for very slipping systems (when the $b_{\mathrm{eff}} H$ term dominates). It will be thus useful to explore the different M_{to} contributions studying how do they compare to H.

3.3 About enthalpy excess and its comparison with the thermo-osmotic response

Let's explore the effect of wetting on the enthalpy excess (per unit area) and how it compares to the predicted thermo-osmotic response coefficient. Because ions are depleted from the wall, wall-ions interactions are almost negligible and wetting mostly affects the water enthalpy excess density profiles, δh_{wat}. As detailed in Section 2, we controlled the wetting by varying the liquid-solid interaction energy $\varepsilon_{\mathrm{LS}} = \{0.160, 0.231, 0.323, 0.416, 0.568\}$ kcal/mol, corresponding respectively to contact angles $\theta \sim \{140°, 130°, 110°, 90°, 50°\}$. In Fig. S4a we can observe the enthalpy excess density profile for different contact angles. We see that δh_{wat} vanishes in the bulk and in the wall region, and that it presents strong oscillations close to the interface, which are more pronounced for the more hydrophilic situations. In Fig. S4b we can see the running integral of the δh_{wat} profiles presented in Fig. S4a. We observe that H_{wat} converges in the bulk region for all the wettings, and that it recovers the strong oscillations at the interface present in δh_{wat}.

The water enthalpy values represented in Fig. S5a are obtained by considering a semi-

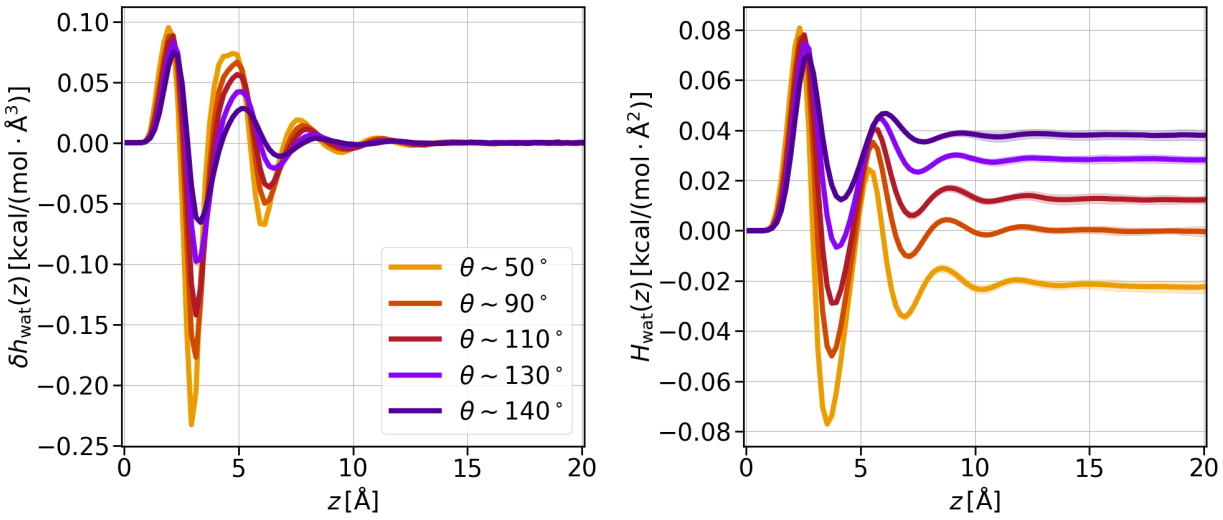

(a) (b)

Figure S4: (a) Enthalpy density profiles for different wettings. (b) Enthalpy excess running integral for different wettings with the same legend as in Fig. S4a.

infinite system constituted by a wall and a homogeneous bulk region far from the interface. We can do so by splitting δh_{wat} profiles in two (one for each wall) and extending the bulk value to infinite. The enthalpy excess is then measured from Eq. (40) with z_0 related to the effective slip determined from NEMD simulations (Table S1): $z_0 = 0$ for $\theta \sim \{140°, 130°, 110°, 90°\}$ (slip situation); and $z_0 = -b_{\mathrm{eff}}$ for $\theta \sim 50°$ (stagnant layer situation). In Fig. S5a we observe that the enthalpy excess increases (from -0.02 kcal/molÅ to 0.04 kcal/molÅ) with the wetting and that it changes sign for $\theta \sim 90°$. Nevertheless, it is interesting to note that a stagnant layer can be present for any wetting due to *e.g.* nanoasperities on the surface. This situation is the typical one in experiments, where some defects and bumps are present in the wall due to the difficulty of obtaining perfectly smooth surfaces with experimental techniques. Therefore, it is interesting to study the effect of different stagnant layers sizes (*i.e.* different integral lower boundaries z_0 in Eq. (40)) for all the wettings considered in this study. The values obtained for H_{wat} as a function of b_{eff} for different contact angles are represented in Fig. S5b. In this figure we observe a strong decrease of the water enthalpy of the system when increasing the stagnant layer size (namely $-b_{\mathrm{eff}}$). This is due to the strong oscillations close to the wall of the running integral discussed in Fig. S4b, which significantly

contribute to the H_{wat} integral value. For $\theta \sim 90°$ we observe a significant increase of H_{wat} in the stagnant layer situation ($b_{\text{eff}} < 0$) when compared to the slip situation ($b_{\text{eff}} > 0$). This is due to the very small value obtained for this wetting in the slip situation, related to the H_{wat} change of sign with the contact angle. Aside of this effect, we also observe for this wetting a H_{wat} decrease when increasing the stagnant layer size.

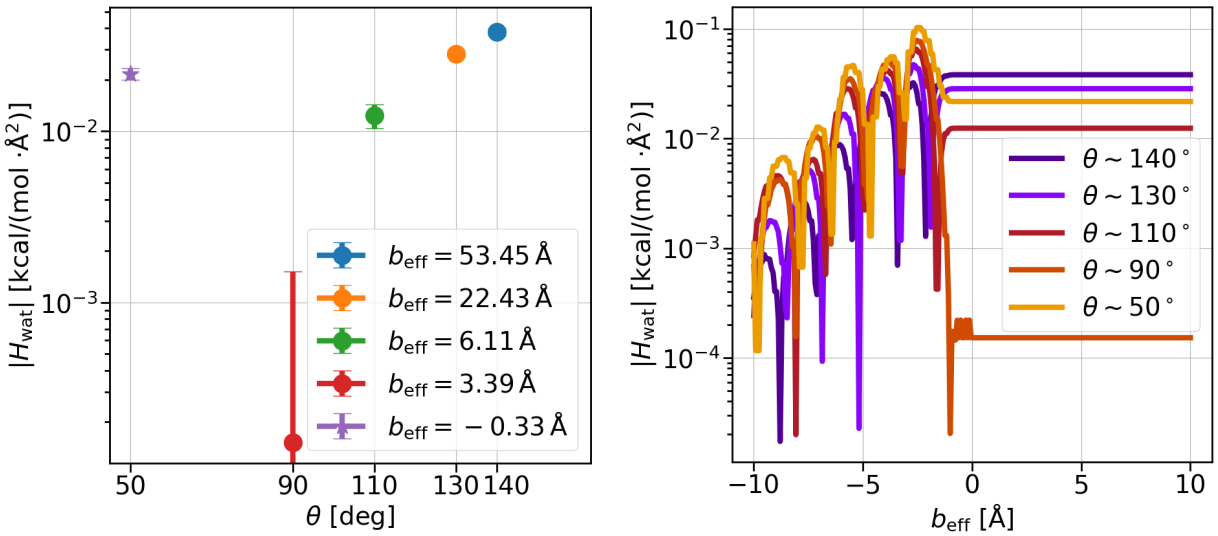

(a) (b)

Figure S5: Enthalpy excess water contribution for different wettings (a) measured for a given effective slip determined from NEMD, stars correspond to $H_{\text{wat}} < 0$ and circles to $H_{\text{wat}} > 0$; (b) as a function of the effective slip b_{eff}. The oscillations for $b_{\text{eff}} < 0$ are due to the oscillations of the enthalpy density profile close to the wall.

With regard to the thermo-osmotic response coefficient, in Fig. S6a we observe a similar wetting effect in its water contribution, which produces a change of sign in $M_{\text{to}}^{\text{wat}}$ in this case also for a contact angle of $\theta \sim 90°$. In Fig. S6b the value of $M_{\text{to}}^{\text{wat}}$ is represented as a function of the effective slip. We observe that, analogously to H_{wat} in Fig. S5b, the presence of a stagnant layer ($b_{\text{eff}} < 0$) significantly reduces the thermo-osmotic response, up to three orders of magnitude for the most hydrophobic systems. We also observe a small effect of slip ($b_{\text{eff}} > 0$) in the value of $M_{\text{to}}^{\text{wat}}$, due to the contribution $b_{\text{eff}} H_{\text{wat}}$ in Eq. (39) (with H_{wat} constant for $b_{\text{eff}} > 0$, see Fig. S5b). This slip contribution is negligible in the case of $\theta \sim 90°$, because $H_{\text{wat}} \sim 0$ for this case. To simplify the coming discussion, in the following,

when referring to H_{wat} and $M_{\mathrm{to}}^{\mathrm{wat}}$, we will restrict to the values shown in Figs. S5a and S6a respectively, obtained for the b_{eff} values from NEMD simulations.

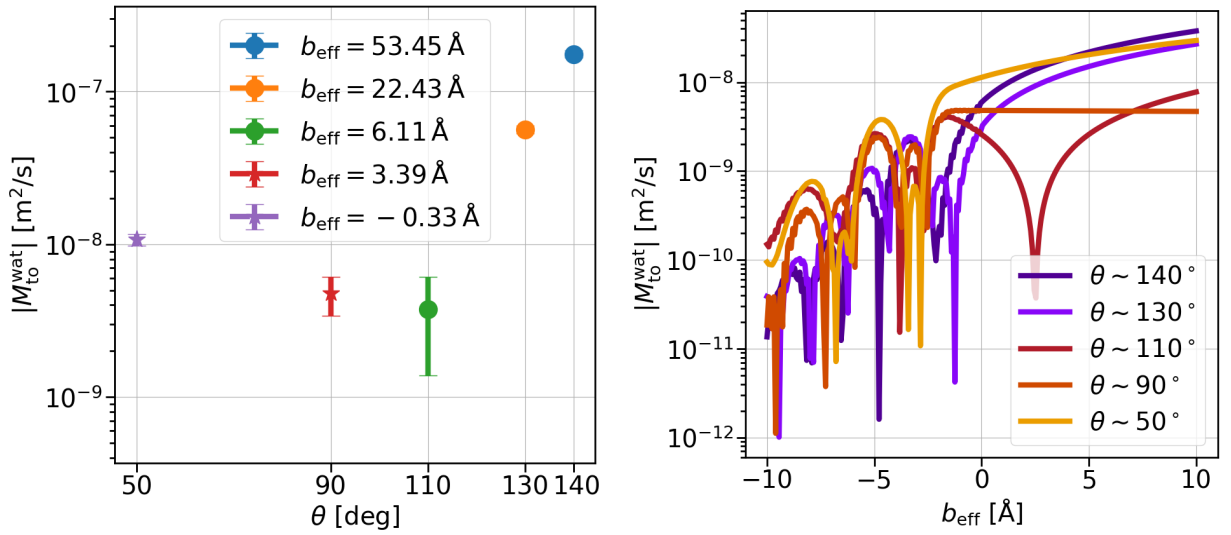

(a) (b)

Figure S6: Thermo-osmotic response coefficient water contribution for different wettings (a) measured for a given effective slip determined from NEMD, stars correspond to $M_{\mathrm{to}}^{\mathrm{wat}} < 0$ and circles to $M_{\mathrm{to}}^{\mathrm{wat}} > 0$; (b) as a function of the effective slip b_{eff}.

The other non-analytical term in Eq. (34) is the one related to the solvation enthalpy of the ions δh_{sol}, defined in Eq. (29). From δh_{sol} we can define H_{sol} and $M_{\mathrm{to}}^{\mathrm{sol}}$, and study how do they compare to the other non-electrostatic and non-analytical term: the water contribution. Because of the depletion of the ionic density profiles from the wall for a neutral surface charge (Fig. S3b), the wetting effect on both H_{sol} and $M_{\mathrm{to}}^{\mathrm{sol}}$ is very small, and the solvation contribution is mostly affected by the Debye length λ_{D} and the surface charge density Σ. We can see in Fig. S7a that, at a given λ_{D}, H_{sol} increases when increasing Σ and that it is not affected by λ_{D} at high Σ, while for low Σ it can vary up to 3 orders of magnitude. In general, we observe that $H_{\mathrm{wat}} \gg H_{\mathrm{sol}}$ for all the λ_{D} and Σ range considered, except for the wetting $\theta \sim 90°$, where the water enthalpy excess is close to 0, and a competition between water and solvation contributions may happen depending on λ_{D} and Σ values. Nevertheless, such competition never happens for the predicted solvation contribution to the thermo-osmotic response coefficient ($M_{\mathrm{to}}^{\mathrm{sol}}$ in Fig. S7b), where for the range of parameters

studied $M_{\rm to}^{\rm wat} \gg M_{\rm to}^{\rm sol}$. Therefore we can consider, in terms of the thermo-osmotic response coefficient, a negligible solvation contribution.

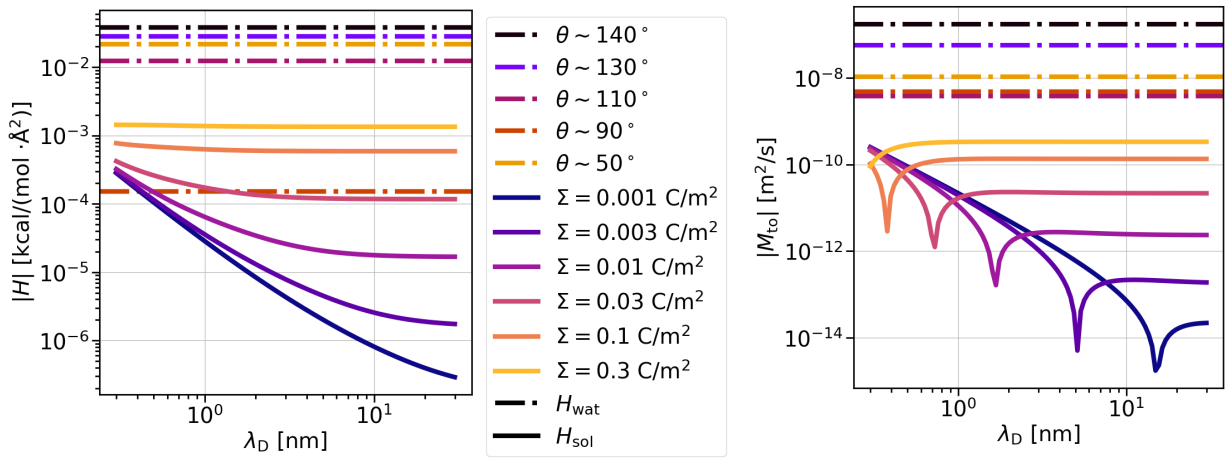

(a) (b)

Figure S7: Comparison between water (dash-dotted lines) and solvation (solid lines) contributions for different wettings θ and different surface charges Σ as a function of the Debye length, respectively for (a) enthalpy excess H; (b) thermo-osmotic response coefficient $M_{\rm to}$.

It is then left to study how the water contribution compares to the electrostatic enthalpy contributions in Eq. (34), namely $\delta h_{\rm dp}$ and $\delta h_{\rm el}^*$ (given by Eqs. (23) and (33) respectively). But first, it is interesting to assess the effect that the consideration of a depletion layer of thickness d_ℓ has in the classical electrostatic term $\delta h_{\rm el}$ (defined in Eq. (13)). With that regard, we can see in Fig. S8 the comparison between the classical and the modified electrostatic terms for the enthalpy excess and the thermo-osmotic response. We observe a similar behavior for H and $M_{\rm to}$, where the electrostatic ($H_{\rm el}$, $M_{\rm to}^{\rm el}$) and modified electrostatic term ($H_{\rm el}^*$, $M_{\rm to}^{\rm el*}$) identify at low Σ and high $\lambda_{\rm D}$. This is because the classical electrostatic potential decays for distances of order of the minimum of $\lambda_{\rm D}$ and $\ell_{\rm GC}$. Then, for the potential to decay for distances larger than d_ℓ (so the depletion layer has a smaller impact in the total integral) it is needed a large $\lambda_{\rm D}$ (or low $n_{\rm s}$) and a large $\ell_{\rm GC}$ (small Σ). In general terms we see that considering the modified electrostatic term implies a decrease of the electrostatic contribution of up to one order of magnitude for the largest Σ considered.

At last, we find represented in Fig. S9 how the modified electrostatic contribution com-

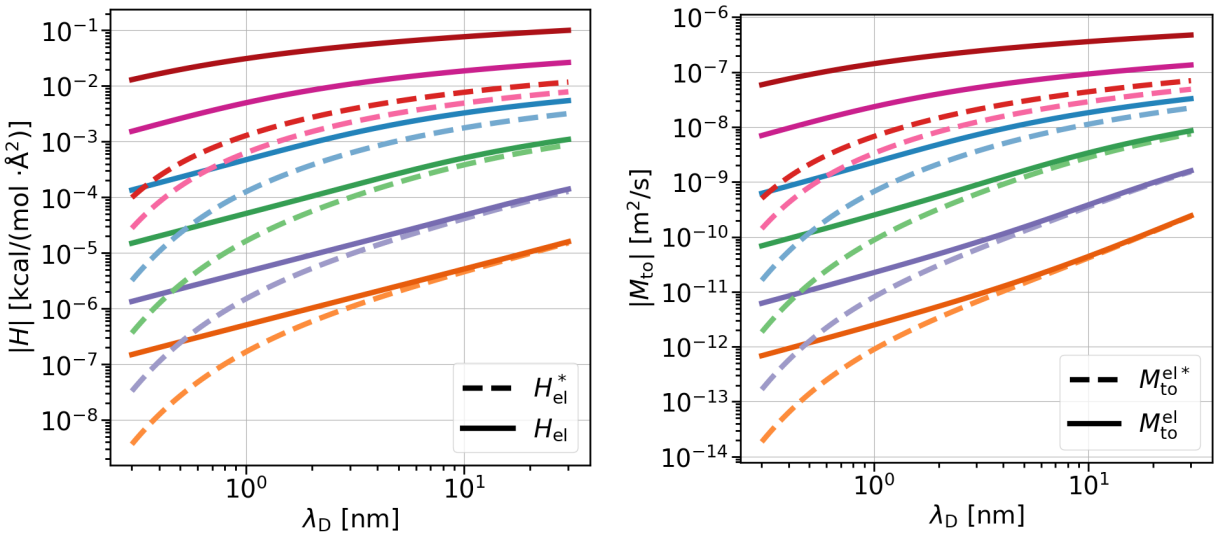

(a) (b)

Figure S8: Comparison between modified electrostatic (dashed lines) and classical electrostatic (solid lines) contributions for different surface charges Σ at a given wetting, as a function of the Debye length, respectively for (a) enthalpy excess H; (b) thermo-osmotic response coefficient M_{to}. The color code is the same as in Fig. S10 (increasing absolute value with increasing surface charge).

pares to the solvent dipole contribution. Again, a similar global behavior is observed for both H and M_{to}. In Fig. S9a, we see that for all Σ and for a broad range of λ_D, $H^*_{el} \gg H_{dp}$, and that both terms are comparable only for the smallest λ_D values considered. In general we see that both contributions increase when increasing λ_D and Σ. We also note that the region where both terms are comparable is when they reach an absolute value smaller than the measured H_{wat} in Fig. S5a, with the exception of $\theta \sim 90°$, when $H_{wat} \sim 0$ and, as we observed also in terms of solvation contribution, a more detailed description is needed for this specific wetting. This detailed description is not required in terms of M_{to} contributions, where we can see, by comparing the water contribution values in Fig. S6a with the ones corresponding to M^{el*}_{to} and M^{dp}_{to} contributions reported in Fig. S9b, that the values for the lower λ_D values where M^{el*}_{to} and M^{dp}_{to} are comparable are much smaller than the reported values of M^{wat}_{to}, on the order of $10^{-8} - 10^{-9}$ m^2/s and thus, we can consider $M^{el*}_{to} \gg M^{dp}_{to}$.

We can hence conclude that the main contributions to the thermo-osmotic response coefficient M_{to} come from the water and the electrostatic term, considering negligible the

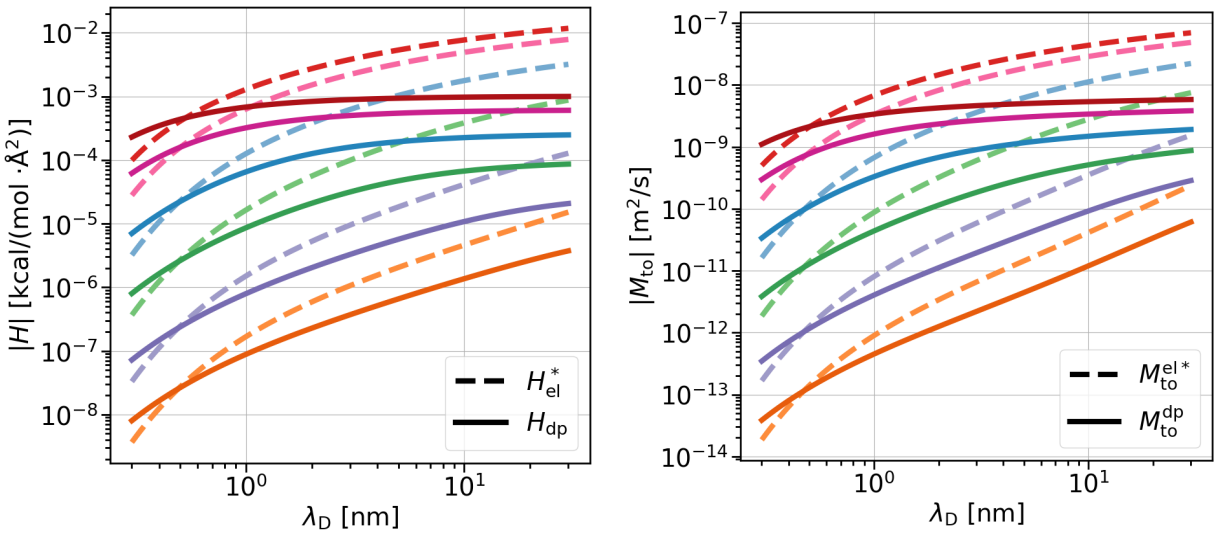

(a) (b)

Figure S9: Comparison between modified electrostatic (dashed lines) and dipole moment (solid lines) contributions for different surface charges Σ at a given wetting, as a function of the Debye length, respectively for (a) enthalpy excess H; (b) thermo-osmotic response coefficient $M_{\rm to}$. The color code is the same as in Fig. S10 (increasing absolute value with increasing surface charge).

solvation and the dipole moment contributions. We can then focus our discussion considering:

$$M_{\rm to} \simeq M_{\rm to}^{\rm wat} + M_{\rm to}^{\rm el*}, \tag{41}$$

and studying how do these contributions affect the total thermo-osmotic response of the system.

4 Thermo-osmotic response results for all wettings

The total thermo-osmotic response coefficient for an aqueous electrolyte consisting on water and a symmetric salt enclosed in between standard Lennard-Jones walls, can be found in Fig. S10.

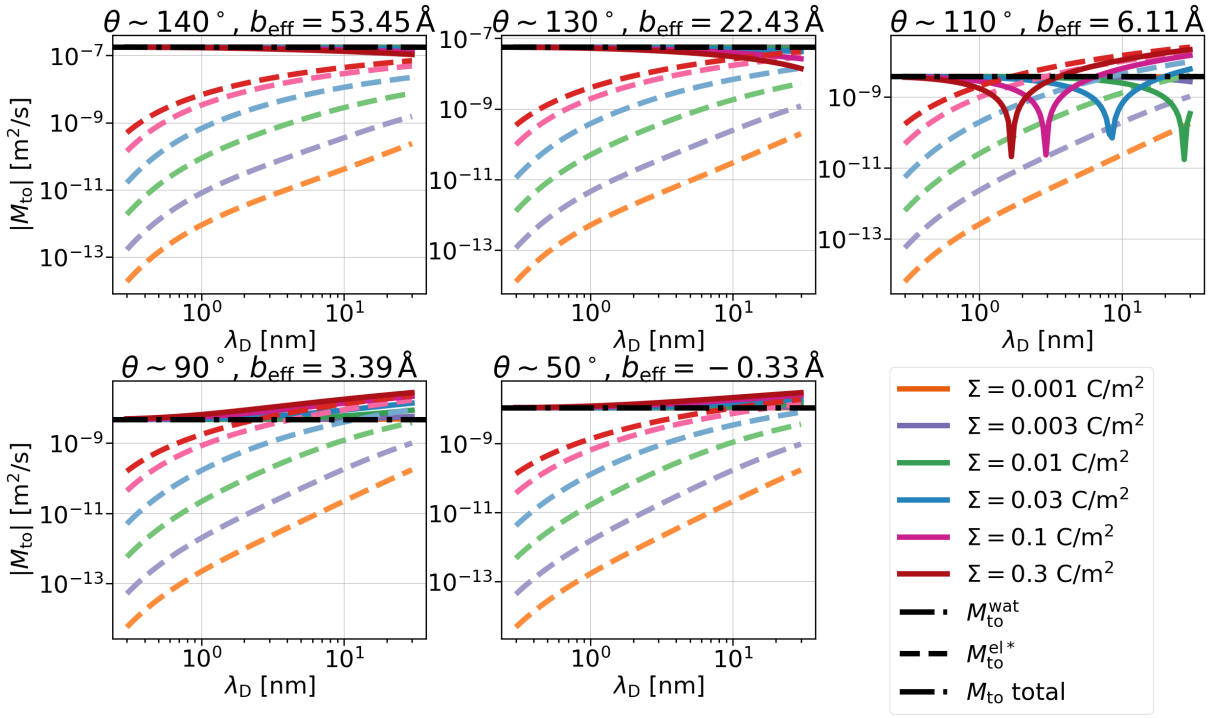

Figure S10: Total thermo-osmotic response coefficient (solid lines) for different wettings and surface charges as a function of the Debye length. In all the graphs the two main contributions, water (dash-dotted lines) and modified electrostatic (dashed lines), are also represented.

References

(S1) Derjaguin, B.; Sidorenkov, G. Thermoosmosis at ordinary temperatures and its analogy with the thermomechanical effect in helium II. *CR Acad. Sci* **1941**, *32*, 622–626.

(S2) Derjaguin, B. V.; Churaev, N. V.; Muller, V. M. *Surface Forces*; Springer, 1987.

(S3) Herrero, C.; Joly, L. Poisson-Boltzmann formulary. *arXiv preprint arXiv:2105.00720* **2021**,

(S4) Herrero, C.; Omori, T.; Yamaguchi, Y.; Joly, L. Shear force measurement of the hydrodynamic wall position in molecular dynamics. *Journal of Chemical Physics* **2019**, *151*.

(S5) Holt, J. K.; Park, H. G.; Wang, Y.; Stadermann, M.; Artyukhin, A. B.; Grigoropou-

los, C. P.; Noy, A.; Bakajin, O. Fast mass transport through sub-2-nanometer carbon nanotubes. *Science* **2006**, *312*.

(S6) Bocquet, L.; Charlaix, E. Nanofluidics, from bulk to interfaces. *Chemical Society Reviews* **2010**, *39*, 1073–1095.

(S7) Secchi, E.; Marbach, S.; Niguès, A.; Stein, D.; Siria, A.; Bocquet, L. Massive radius-dependent flow slippage in carbon nanotubes. *Nature* **2016**, *537*.

(S8) Fu, L.; Merabia, S.; Joly, L. What Controls Thermo-osmosis? Molecular Simulations Show the Critical Role of Interfacial Hydrodynamics. *Physical Review Letters* **2017**, *119*, 214501.

(S9) Bregulla, A. P.; Würger, A.; Günther, K.; Mertig, M.; Cichos, F. Thermo-Osmotic Flow in Thin Films. *Physical Review Letters* **2016**, *116*, 1–5.

(S10) Ganti, R.; Liu, Y.; Frenkel, D. Molecular Simulation of Thermo-osmotic Slip. *Physical Review Letters* **2017**, *119*, 1–5.

(S11) Oyarzua, E.; Walther, J. H.; Megaridis, C. M.; Koumoutsakos, P.; Zambrano, H. A. Carbon Nanotubes as Thermally Induced Water Pumps. *ACS Nano* **2017**, *11*, 9997–10002.

(S12) Fu, L.; Merabia, S.; Joly, L. Understanding Fast and Robust Thermo-osmotic Flows through Carbon Nanotube Membranes: Thermodynamics Meets Hydrodynamics. *The Journal of Physical Chemistry Letters* **2018**, *9*, 2086–2092.

(S13) Mengual, J. I.; Aguilar, J.; Fernandez-Pineda, C. Thermoosmosis of water through cellulose acetate membranes. *Journal of Membrane Science* **1978**, *4*, 209–219.

(S14) Derjaguin, B. V. Structural And Thermodynamic Peculiarities Of The Boundary Layers Of Liquids. *Pure and Applied Chemistry* **1980**, *52*.

(S15) Rusconi, R.; Isa, L.; Piazza, R. Thermal-lensing measurement of particle thermophoresis in aqueous dispersions. *Journal of the Optical Society of America B* **2004**, *21*.

(S16) Nedev, S.; Carretero-Palacios, S.; Kühler, P.; Lohmüller, T.; Urban, A. S.; Anderson, L. J.; Feldmann, J. An optically controlled microscale elevator using plasmonic janus particles. *ACS Photonics* **2015**, *2*.

(S17) Huang, D. M.; Cottin-Bizonne, C.; Ybert, C.; Bocquet, L. Aqueous Electrolytes near Hydrophobic Surfaces: Dynamic Effects of Ion Specificity and Hydrodynamic Slip. *Langmuir* **2008**, *24*, 1442–1450.

(S18) Fu, L.; Joly, L.; Merabia, S. Giant Thermoelectric Response of Nanofluidic Systems Driven by Water Excess Enthalpy. *Physical Review Letters* **2019**, *123*, 1–15.

(S19) Plimpton, S. Fast parallel algorithms for short-range molecular dynamics. *Journal of Computational Physics* **1995**, *117*.

(S20) Berendsen, H. J.; Grigera, J. R.; Straatsma, T. P. The missing term in effective pair potentials. *Journal of Physical Chemistry* **1987**, *91*, 6269–6271.

(S21) Huang, D. M.; Cottin-Bizonne, C.; Ybert, C.; Bocquet, L. Ion-specific anomalous electrokinetic effects in hydrophobic nanochannels. *Physical Review Letters* **2007**, *98*, 1–4.

(S22) Koneshan, S.; Rasaiah, J. C.; Lynden-Bell, R. M.; Lee, S. H. Solvent structure, dynamics, and ion mobility in aqueous solutions at 25 °C. *Journal of Physical Chemistry B* **1998**, *102*, 4193–4204.

(S23) Bett, K. E.; Cappi, J. B. Effect of pressure on the viscosity of water [1]. 1965.

(S24) Harris, K. R.; Woolf, L. A. Temperature and volume dependence of the viscosity of water and heavy water at low temperatures. *Journal of Chemical and Engineering Data* **2004**, *49*.

(S25) Werder, T.; Walther, J. H.; Jaffe, R. L.; Halicioglu, T.; Koumoutsakos, P. Erratum: On the water-carbon interaction for use in molecular dynamics simulations of graphite and carbon nanotubes (Journal of Physical Chemistry B (2003) 107B (1349)). *Journal of Physical Chemistry B* **2008**, *112*, 14090.

(S26) Hafskjold, B.; Ikeshoji, T. Microscopic pressure tensor for hard-sphere fluids. *Physical Review E - Statistical Physics, Plasmas, Fluids, and Related Interdisciplinary Topics* **2002**, *66*, 11203.

(S27) Kusaka, I. Statistical Mechanics of Inhomogeneous Fluids. *Statistical Mechanics for Engineers* **2015**, *379*, 259–308.

(S28) Ganti, R.; Liu, Y.; Frenkel, D. Hamiltonian Transformation to Compute Thermo-osmotic Forces. *Physical Review Letters* **2018**, *121*, 68002.